



MIT Open Access Articles

Design Drivers of Energy-Efficient Transport Aircraft

The MIT Faculty has made this article openly available. **Please share** how this access benefits you. Your story matters.

Citation	Drela, Mark. Design Drivers of Energy-Efficient Transport Aircraft. Warrendale, PA: SAE International, 2011.
As Published	http://dx.doi.org/10.4271/2011-01-2495
Publisher	SAE International
Version	Author's final manuscript
Citable link	http://hdl.handle.net/1721.1/86398
Terms of Use	Creative Commons Attribution-Noncommercial-Share Alike
Detailed Terms	http://creativecommons.org/licenses/by-nc-sa/4.0/

Design Drivers of Energy-Efficient Transport Aircraft

Mark Drela

MIT Department of Aeronautics and Astronautics, Cambridge, MA 02139

The fuel energy consumption of subsonic air transportation is examined. The focus is on identification and quantification of fundamental engineering design tradeoffs which drive the design of subsonic tube and wing transport aircraft. The sensitivities of energy efficiency to recent and forecast technology developments are also examined.

Background and Motivation

Early development of the modern jet transport, starting with the DeHavilland Comet and Boeing 707 in the 1950's, was strongly driven by range requirements. With the imperatives of rising fuel costs and increased environmental concerns, more recent developments have focused on fuel economy and also on noise. Of the three main drivers of fuel economy — aerodynamics, structures, and propulsion — the latter has seen the largest improvements, not surprisingly because in the 1950's turbojet and turbofan engines were a very young technology. As engine technology maturation has now reached the levels of the other disciplines, further improvements will have to come from all technologies. The recent and ongoing NASA Aeronautics research,¹ in particular the N+1,2,3 programs² target a wide range of aerodynamic, structural, and propulsion technologies towards this goal.

The objective of this document is to identify the major competing effects which influence the design parameters of a tube and wing transport aircraft, optimized for minimum fuel burn. Sensitivities of fuel burn to the following parameters will be determined and presented:

- flight Mach number
- allowable specific stress and load factor
- allowable turbine metal temperatures
- engine overall pressure ratio
- balanced field length
- stability margin

Recent configuration technologies from the N+3 program will also be mentioned.

The main focus will be on short to medium-range Boeing 737 or Airbus A320 class aircraft, since this is one of the largest air travel market segments. Longer range aircraft in the Boeing 777 or Airbus A340 class will also be examined for a few cases.

The overall objective is to identify which parameters or combinations of parameters have the greatest potential for enabling fuel burn reductions, and therefore are the most attractive targets for research and development.

Fuel Consumption Overview

We will begin by examining the major overall factors which contribute to fuel burn, via the Breguet relation. This analysis is too coarse to provide any useful design guidance, but it does help to interpret some possibly counterintuitive results from much more detailed optimization results presented later.

Fuel consumption via Breguet relation

The fuel weight W_{fuel} consumed to fly a distance (range) R by an aircraft in level flight at Mach number M is given by the Breguet relation.

$$W_{\text{fuel}} = W_{\text{ZF}} \left[\exp\left(\frac{D}{L} \frac{TSFC}{M} \frac{R}{a}\right) - 1 \right] \quad (1)$$

$$\simeq W_{\text{ZF}} \times \frac{D}{L} \times \frac{TSFC}{M} \times \frac{R}{a} \quad (2)$$

The exact and linearized forms (1),(2) are compared in Figure 1 for a typical modern jet transport. Long range missions in effect get progressively more penalized for carrying the extra fuel. The linearized form

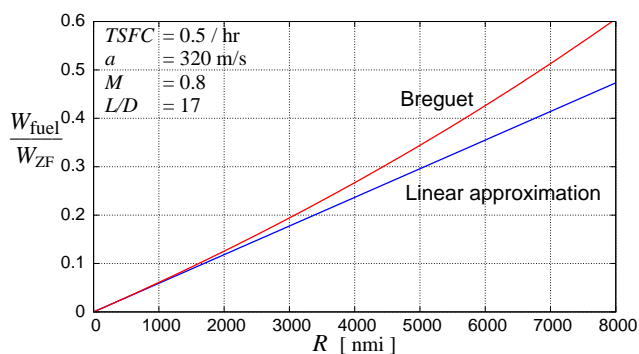


Fig. 1 Fuel weight fraction versus mission range for a typical jet transport. The linear approximation is valid for short to medium range missions.

shows that the fuel weight is approximately the product of three parameters:

- W_{ZF} Zero-fuel weight (at landing).
- D/L Drag/lift ratio.
- $TSFC/M$ Thrust-specific fuel consumption over Mach

The range R is fixed by the mission and the speed of sound a at cruise altitude is a physical constant, and hence these are not design variables. In the limit of

very high-bypass ratio engines or lightly-loaded propellers, the $TSFC$ scales nearly as the cruise Mach M . In this situation the ratio $TSFC/M$, which is equivalent to a power-specific fuel consumption, is the relevant measure of propulsion-system efficiency. For a fixed-parameter turbofan engine, the ratio $TSFC/M^{0.5}$ stays roughly constant with M , while for an optimized engine the ratio $TSFC/M^{0.7}$ is roughly constant. The corresponding aerodynamic figures of merit for the two approaches are then $M^{0.5}L/D$ and $M^{0.3}L/D$, respectively. Which approach is chosen is largely a matter of preference when performing manual parametric studies. The choice is immaterial for the parameter studies presented here, since the engine is simulated directly, for any given M , without reliance on any assumed empirical $TSFC$ vs. M dependency.

Although equations (1) and (2) correctly give the fuel burn, they are nearly useless as a design guide. The reason is that any one of the three parameters can be reduced in isolation, but this will generally increase the others. For example, D/L can be reduced by increasing the wing aspect ratio or the wing/wetted area fraction, but this will be offset by an increase in the wing weight's contribution to W_{ZF} . The $1/M$ factor can be decreased by choosing to fly faster, but this will increase all the other factors and actually give a net increase in the fuel burn. Since all the factors influence each other to varying degrees, to minimize fuel burn it is essential to account for their important interactions and tradeoffs. This is addressed by the conceptual-design approach, whose application is the central focus of this paper.

Fuel burn and flight altitude

From the most fundamental viewpoint, the objective of air transportation is to move the fuselage — in effect a payload container — over a required range R , at an economically-viable speed or Mach number, with the smallest fuel weight or more generally energy expenditure. The latter is quantified by the Payload-Fuel Energy Intensity ($PFEI$),³

$$PFEI \equiv \frac{h_{\text{fuel}} W_{\text{fuel}}}{W_{\text{pay}} R} \quad [\text{kJ/kg km}] \quad (3)$$

$$= \frac{\text{Fuel energy}}{\text{Payload mass} \times \text{Distance}}$$

where h_{fuel} is the fuel specific heating value. This allows an energy-usage efficiency comparison between different aircraft and mission lengths, between different fuels, and between different modes of transportation (air, land, water).

To examine a transport aircraft's energy requirements in this framework, expression (2) is recast by separating the components of the drag D , assuming $W_{ZF} \simeq L$, and defining an effective power specific fuel consumption based on thrust power $PSFC_T \equiv$

$TSFC/V$.

$$PFEI \simeq (D_{\text{fuse}} + D_{\text{rest}} + D_i) PSFC_T \frac{h_{\text{fuel}}}{W_{\text{pay}}} \quad (4)$$

The absolute minimum energy required to transport the fuselage is

$$PFEI_{\text{min}} = D_{\text{fuse}} PSFC_T \frac{h_{\text{fuel}}}{W_{\text{pay}}} \quad (5)$$

with the energy consumed by the induced drag and the profile drag of the remaining components being in effect “overhead”. D_{fuse} and the corresponding $PFEI_{\text{min}}$ can be quantified via the usual average skin friction, form factor, and wetted area, as described by Shevell.⁴

$$PFEI_{\text{min}} = \frac{\gamma}{2} p M^2 C_{f_{\text{wet}}} F_f A_{\text{wet}} PSFC_T \frac{h_{\text{fuel}}}{W_{\text{pay}}} \quad (6)$$

The dynamic pressure has also been replaced by the static pressure p and flight Mach number by the relation $\rho V^2 = \gamma p M^2$.

The effect of Mach number will be examined in detail later. If this is considered fixed, then aside from reduced $C_{f_{\text{wet}}}$ via riblets or laminar flow⁵ (which will also be examined later), the only variable in (6) which can be freely varied to significantly reduce $PFEI_{\text{min}}$ is the pressure p at cruise altitude. Indeed, transportation of the fuselage is “free” if performed at extreme altitudes where $p \simeq 0$. But of course an increase in flight altitude adds more “overhead” in the form of larger and heavier surfaces and engines, whose profile and induced drag add to the full fuel energy expression (4). This tradeoff is quantified in Figure 2. The

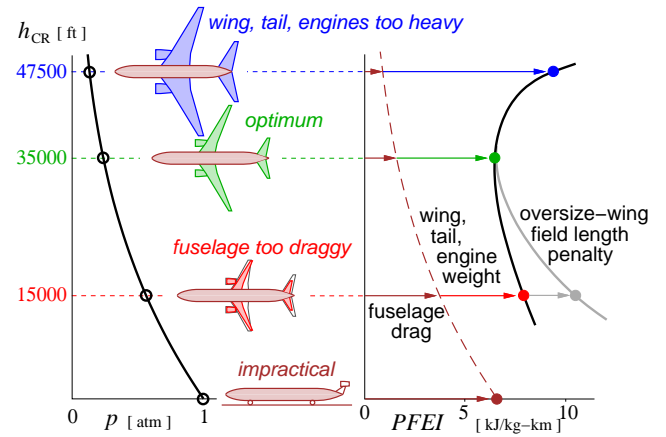


Fig. 2 Mission fuel-energy use versus cruise altitude for a jet transport with a B737-class fuselage, at fixed cruise Mach $M_{\text{CR}} = 0.8$. Lower pressure at altitude decreases fuel burn from fuselage drag, but increases fuel burn from “overhead” of wings, tails, engines.

optimum altitude for any given Mach number is where the fuel burn due to fuselage drag and due to overhead have equal and opposite sensitivity to pressure.

It's interesting (if not amusing) to consider transporting the fuselage at sea level as a wheeled vehicle, since this eliminates the weight and drag overhead of the wings and tails, and also eliminates induced drag. As indicated in Figure 2, the energy required to do this is actually comparable to the energy needed to fly the fuselage at the optimum altitude at the same Mach number. Needless to say, a wheeled fuselage traveling overland at $M=0.8$ is not practical.

Transport Aircraft Design Space

Conceptual design formulations

At the detail-design level, a vast number of parameters is needed to fully define an aircraft, its engines, and its operation. A major goal of the initial conceptual design stage is to greatly reduce the number of parameters by some combination of historical correlations and low-order modeling, and thus allow initial sizing and optimization.

Because aircraft fuel burn depends on many competing drivers, any effective conceptual design formulation must retain the key features of all the disciplines involved. As a minimum, the airframe structure and weights, the aerodynamic performance, the propulsion performance, and the flight trajectory must all be represented with sufficient fidelity. Many conceptual design approaches have been developed towards this end, e.g. by Roskam,⁶ Torrenbeek,⁷ Raymer,⁸ Jayaram,⁹ Mason,¹⁰ and others.

Conceptual design methods more focused on formal optimization have also been developed. These are commonly referred to as Multi-Disciplinary Optimization, or MDO methods. Examples are the methods of Knapp,¹¹ Wakayama,¹² and Kroo.¹³ The author's TASOPT formulation¹⁴ also falls into this class.

TASOPT Summary

Because TASOPT was used to generate the key results in this paper, a brief summary is given here so the fidelity as well as limitations of the results can be better understood. TASOPT uses first-principles methods for its primary weight, aerodynamic, and engine performance predictions. Specifically, it uses

- Beam and pressure-vessel theory for primary-structure sizing and weight prediction, Figure 3.
- Variable wing airfoils and viscous/inviscid CFD for all profile drag prediction, Figure 4.
- Full engine flowpath simulation, Figure 5.
- Variable flight trajectory, Figure 6.

Significantly, TASOPT does not rely on historical primary-structure weight correlations, wetted-area drag prediction methods, engine lookup tables or correlations, or fixed climb and cruise profiles. The minimal reliance on historical data and empiricism

gives considerable confidence in the design parameter sweeps presented here, even if they go into uncharted territory. For more detailed TASOPT documentation and validation see Drela¹⁴ and Greitzer.¹⁵

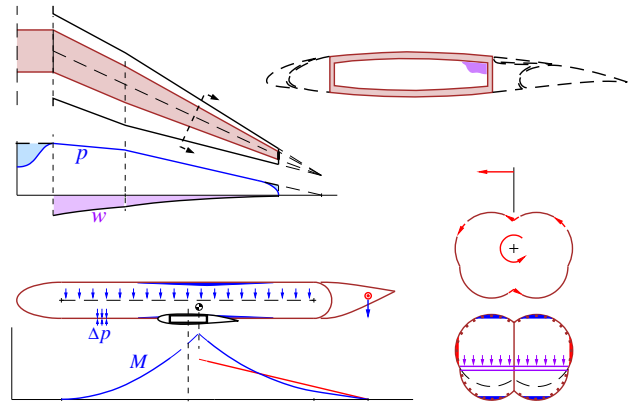


Fig. 3 TASOPT structural and weight models for wing and fuselage, based on simple beam and pressure-vessel theory.

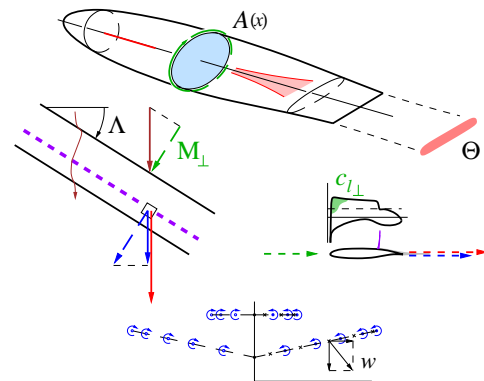


Fig. 4 TASOPT wing and fuselage profile drag models, and Trefftz-Plane induced drag model.

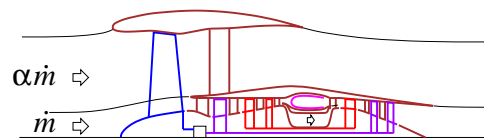


Fig. 5 TASOPT turbofan engine performance model. The entire flowpath is simulated, including the effects of turbine cooling flow.

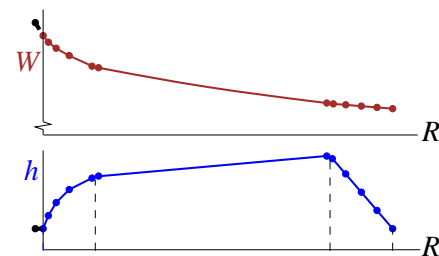


Fig. 6 TASOPT trajectory simulation for takeoff performance and mission fuel burn.

Design closure and optimization

For any given set of *model parameters*, design closure is the convergence of all the derived model quantities towards a self-consistent design. Such a “closed” design meets all structural criteria, and also mission requirements such as range, takeoff distance, and climb gradient. Optimization can then be performed around this closure procedure. In TASOPT this is implemented as two nested loops, shown in Figure 7.

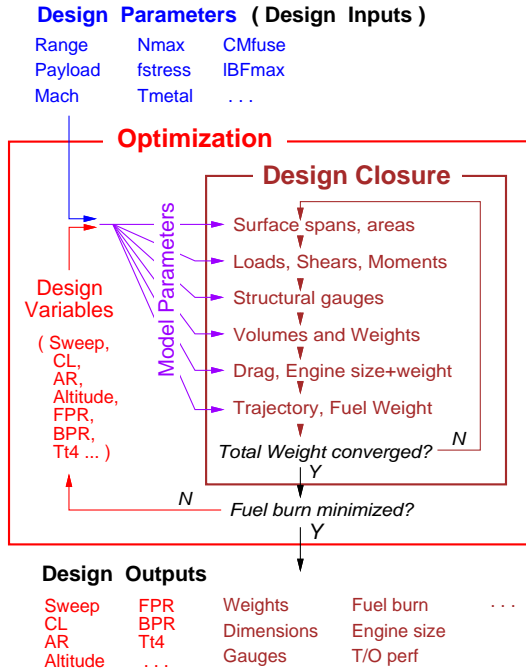


Fig. 7 TASOPT design-closure and optimization procedure. The Model Parameters required by the inner closure loop are partitioned into the Design Parameters which are explicitly specified, and Design Variables which are calculated by the outer optimization loop.

Design variable subset

Of the 100 or so model parameters required to define the aircraft at the conceptual level, a much smaller subset is eligible for use as *design variables* in the outer loop. These are the model parameters which have a non-monotonic influence on the fuel-burn design objective, and hence must be determined via optimization if the optimum aircraft is to be obtained. The remaining model parameters are the *design parameters*, and are typically set to the best-available values limited by technology, with some allowance for cost.

Table 1 gives the complete list of the design variables used in the TASOPT formulation. The $()_i$ index goes over some number of spanwise stations, so that λ_i define the planform shape, and $\lambda_i r_{c_{\ell_i}}$ define the spanwise-loading shape.

Importance of global optimization

A major focus of this paper is the quantification of fuel burn versus a number of key design parameters re-

Table 1 Design variables determined by global mission optimization.

$C_{L_{CR}}$	cruise lift coefficient
AR	aspect ratio
Λ	wing sweep angle
λ_i	section relative chords (taper ratios)
$(t/c)_i$	section airfoil thicknesses
$r_{c_{\ell_i}}$	section local/root c_{ℓ} ratios
FPR_D	design fan pressure ratio
BPR_D	design bypass ratio
$T_{t4_{TO}}$	turbine inlet temperature at takeoff
$T_{t4_{CR}}$	turbine inlet temperature in cruise
h_{CR}	start-of cruise altitude

lated to technology. An essential feature of this study is that for any set of input design parameters (at the top of Figure 7), the fuel burn of the optimized aircraft is taken as the figure of merit.

The importance of this continuous optimization is illustrated in Figure 8. If the cruise Mach number of the

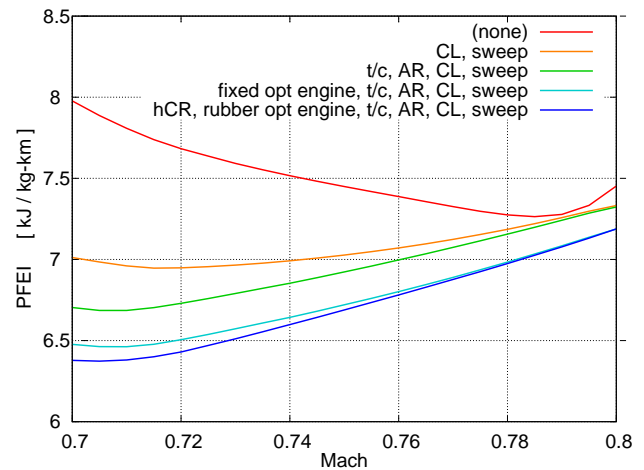


Fig. 8 Fuel burn versus cruise Mach, for different optimization design variable sets. Expanding the design set reduces the minimum fuel burn, and also changes the optimum cruise Mach.

baseline B737 is reduced, and all the other model parameters are held fixed, the result is an increase in the fuel burn as indicated by the topmost line in Figure 8. As more and more model parameters are included in the optimized design variable set, however, then progressively larger fuel savings are obtained with the slower cruise. The greatest fuel reduction occurs if all the variables listed in Table 1 are optimized. Clearly, optimizing the entire aircraft+engine+operation system is necessary to obtain the true design-parameter sensitivity, with respect to Mach number in this case. Such full optimization will be used for the subsequent sensitivity studies, so that the results represent the greatest possible fuel savings from a change in each design parameter being considered.

Design Parameter Sensitivities

The subsequent sections show the optimum-aircraft fuel burn sensitivity with respect to key design parameters. These are chosen based both on their influence on fuel burn in potential future aircraft, and on their strong dependence on technology. The results can be interpreted as a guide to research investment for future aircraft, in that they quantify the potential fuel-economy payoff of the parameters being examined.

Two baseline aircraft will be examined: a medium range aircraft in the Boeing 737 or Airbus A320 class, and a long range aircraft in the Boeing 777 or Airbus A340 class. Their specified key parameters are listed in Table 2, and will be held fixed except where stated otherwise. The payloads correspond to 180 and 500 all-economy passengers, respectively. Since the range and payload are fixed, W_{fuel} and $PFEI$ are effectively equivalent. The fuel burn will also be given as a ratio from the baseline, to more easily see the potential fuel savings as a percentage.

Table 2 Key parameters of baseline aircraft.

	B737-class	B777-class
Fuse.OML	737-800	777-300ER
Payload	37 000 lb	115 000 lb
Range	3000 nmi	6500 nmi
Mach	0.80	0.84
Field	8000 ft	9500 ft

Although the fuselage outer mold lines are held fixed, the wing and tail surfaces are always sized and wing is positioned based on required-lift, trim, and stability requirements. All structural gauges are likewise always sized via specified load conditions and material properties. Conventional aluminum materials are assumed. Engines are sized for the cruise-thrust condition, under the constraint of a minimum specified balanced field length and minimum climb gradient.

Cruise Mach number

A reduced cruise Mach number has previously been considered as a means for reducing mission fuel burn.² One drawback of the reduced speed is a negative impact on airline productivity and passenger acceptance, especially for long-range missions. For short-to medium-range aircraft, however, the flight-time increase is less problematic thus making slower cruise an attractive possibility.

Figure 9 shows the relative fuel burn and other parameters of interest for a B737-class aircraft for a range of specified cruise Mach numbers. The plots show a “rubber system” spectrum, with each point on the horizontal axis representing a different airplane, engine, and flight profile combination, all optimized together for that Mach number. Optimization was performed with and without a span constraint, since a span increase has implications on compatibility with existing airport infrastructure.

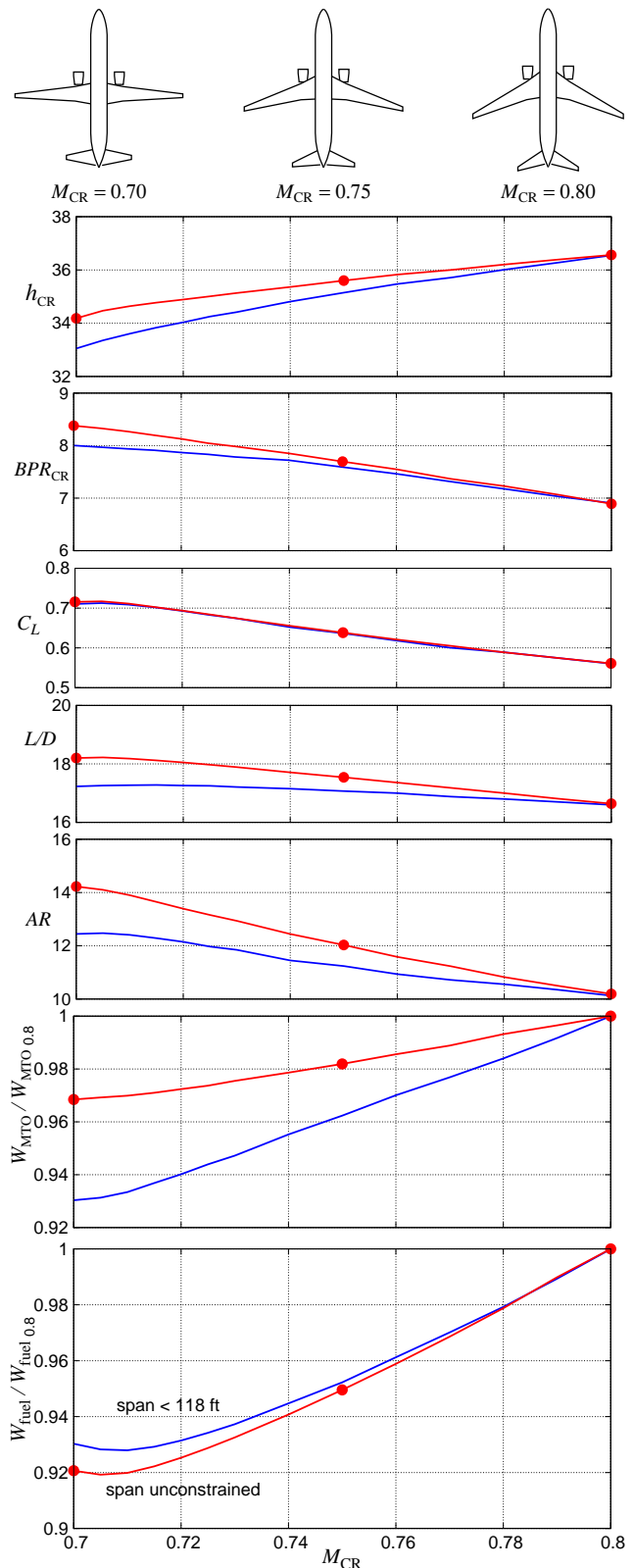


Fig. 9 Optimum B737-class aircraft parameters versus design cruise Mach.

The three sketches at the top of Figure 9 show three airplane geometry instantiations for the three $M_{CR} = 0.7, 0.75, 0.8$ values. The optimization procedure chose the wing sweep angle shown, along with all the other

design variables listed in Table 1. Also, the inside design-closure loop shown in Figure 7 generated all the key airframe gauges and engine parameters in the optimization process.

As the cruise Mach number M_∞ is reduced the optimum sweep angle Λ is also reduced, roughly according to the infinite swept wing relation

$$\cos \Lambda \simeq \frac{M_{\text{crit}}}{M_\infty} \quad (7)$$

where M_{crit} is in the range 0.70 ... 0.75 for modern transonic airfoils, depending on the airfoil thickness t/c and the local lift coefficient. Relation (7) indicates that as $M_\infty \rightarrow M_{\text{crit}}$, then $\cos \Lambda \rightarrow 1$ and the sweep angle tends to approach zero. As the sweep is reduced, the optimum aspect ratio AR will then tend to increase as allowed by the reduction of structural span for a given aerodynamic projected span.

The engine parameters also change significantly, with the cruise-condition bypass ratio BPR_{CR} increasing notably as M_{CR} decreases. A major reason is that the fan face always requires a fixed local $M_{\text{fan}} \simeq 0.6$, so a lower cruise Mach results in a smaller required diffusion $M_{\text{CR}} - M_{\text{fan}}$. The less-loaded nacelle then has smaller superelevations on its outside surface, as shown in Figure 10. This mitigates the nacelle profile drag penalty of a large-diameter fan, and thus the system optimizes to a larger bypass ratio.

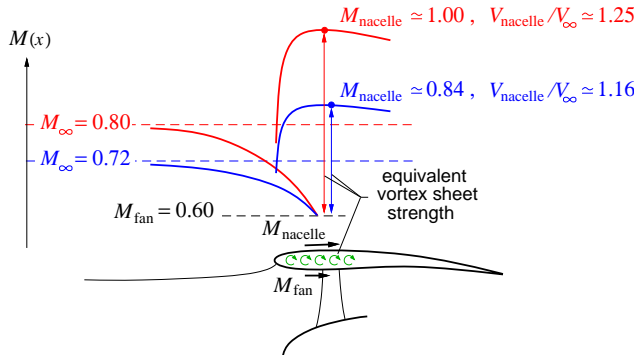


Fig. 10 With a fixed fan-face Mach number, the nacelle’s external superelevations decrease disproportionately as cruise Mach number is reduced.

Somewhat less obvious is the decrease in the optimum start-of-cruise altitude h_{CR} . An explanation is provided by the previous fuel burn versus altitude tradeoff shown in Figure 2. The reduced Mach number decreases the minimum-possible fuel burn $PFEI_{\text{min}}$ as given by (6), so that it is less imperative to fly high to reduce it. This shrinks the wing and engines and their “overhead” weight and nacelle drag. The takeoff distance is still acceptable since reduced wing sweep naturally increases the achievable $C_{L_{\text{max}}}$.

The span constraint in Figure 9 is seen to have a strong effect on the overall L/D and the gross weight $W_{\text{MTO}} = W_{\text{ZF}} + W_{\text{fuel}}$. However, these two quantities

have a directly opposite effect on the fuel burn W_{fuel} , as can be seen in the Breguet relation (2), so that the net effect on fuel burn is remarkably small. This weak dependence on span will also be evident in the other parameter sensitivity results shown later.

The results in Figure 9 were computed assuming a fixed minimum static stability margin $SM_{\text{min}} = 0.15$. If this value is strongly driven by pitch-up associated with transonic stall, then the SM_{min} value can likely be decreased along with the reduced cruise Mach. The additional fuel-burn benefit from this reduced SM_{min} will be examined later.

Material Strength/Weight

Stronger airframe materials have of course always been the subject of intense research and development. One result has been the relatively recent introduction of composites into the primary structure of the Boeing 787 and to some extent the Airbus A380.

Development of advanced sensor technology and data acquisition capabilities has enabled the possibility of Structural Health Monitoring (SHM)¹⁶ to be used on aircraft in routine service, which could allow reductions in allowables since less margin is needed for unanticipated corrosion, fatigue cracking, and impact damage. The latter is of particular interest for composite airframes.

Here we will examine the *maximum possible* fuel burn reductions resulting from increased allowable material stress, representing either material improvements, or the introduction of SHM. In the context of a conceptual-design model like TASOPT, the only relevant parameter is the material’s allowable-stress/density ratio. Here this is quantified by a simple factor multiplying the baseline value, which here corresponds to standard aluminum.

One question which arises in any such technology improvement is to how to best exploit it. For example, some possible ways to exploit a stronger wing material are:

- larger aspect ratio AR
- smaller airfoil t/c together with smaller sweep Λ
- larger S/A_{wet} and higher cruise

The best-possible solution is likely to be some combination of all these changes, and possibly others which may not be obvious. For example, significantly different engine parameters may be optimal with the higher cruise altitude favored by a relatively lighter material. In TASOPT all these trades are made by its global optimization, so that the resulting aircraft+engine+operation combination takes the best possible advantage of the improved technology.

Figure 11 shows the relative fuel burn and other parameters for the B737-class aircraft for a range of material stress factor. The global optimization was performed with and without a span constraint. As expected, the optimum aspect ratio and resulting cruise

L/D increase with the stronger material, and the overall weight also decreases. The result is a substantial 13% fuel burn reduction for a 50% material stress increase. There is also a 1500 ft increase in the optimum start-of-cruise altitude, since the higher-specific stress material reduces the “overhead” weight cost of a larger wing which is needed to fly higher.

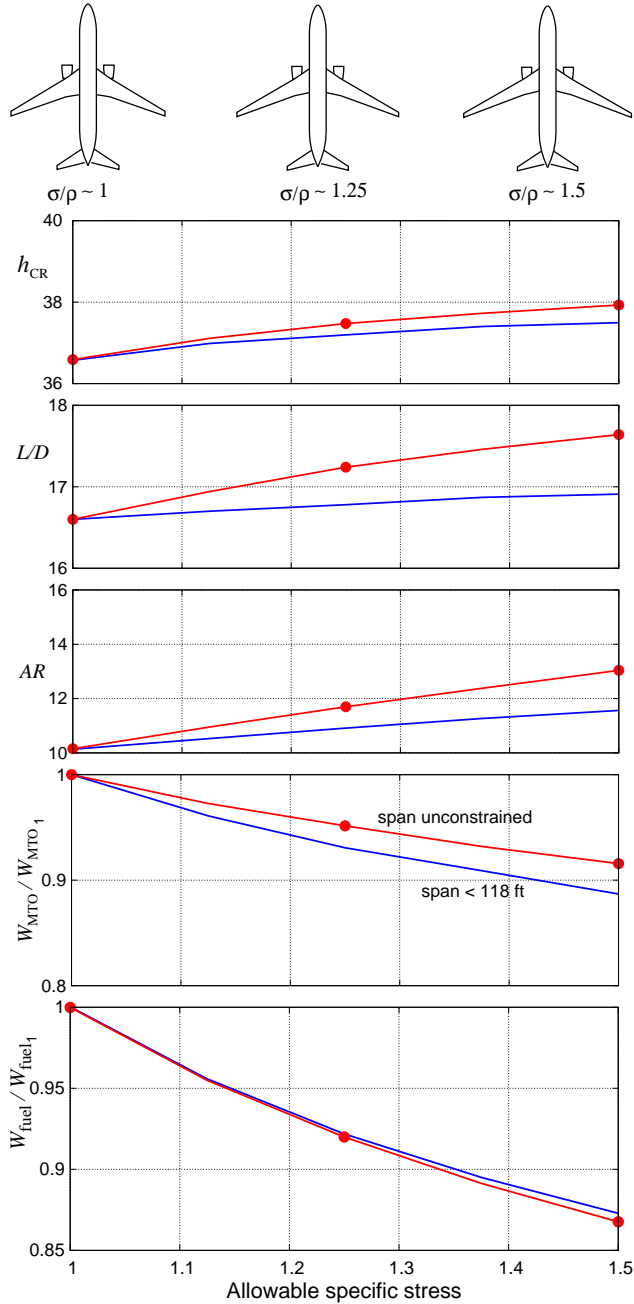


Fig. 11 Optimum B737-class aircraft parameters versus allowable specific stress.

The same sensitivity to material stress has been calculated for the B777-class aircraft, with the results shown in Figure 12. The trends are similar to those for the smaller and shorter-range aircraft, but the sensitivities are considerably greater. Now the 50% specific stress increase gives a very large 20% fuel burn re-

duction, and increases the start-of-cruise altitude by 3000 ft. The larger effect of better material on the B777-class airplane can be attributed to the cube-square law, which dictates that material stress/density has a greater impact on larger structures. Another contributing effect is the Breguet nonlinearity shown in Figure 1.

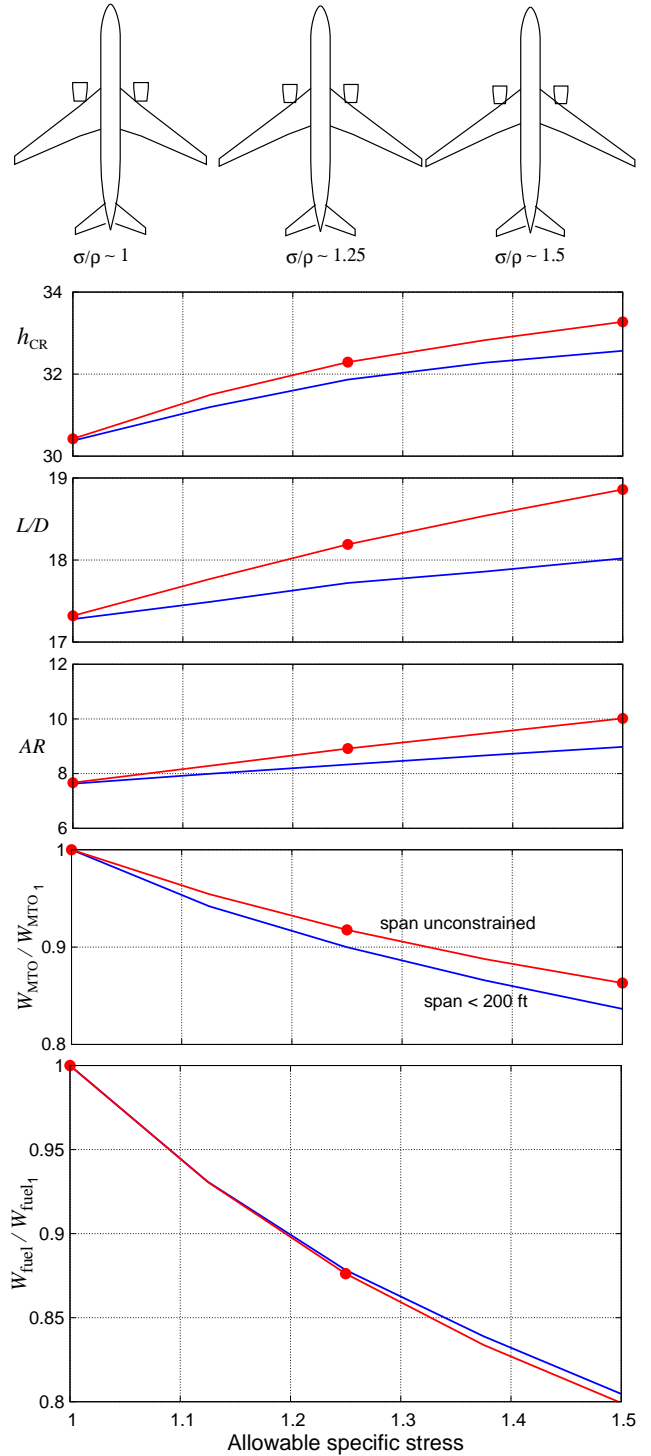


Fig. 12 Optimum B777-class aircraft parameters versus allowable specific stress.

Load factor

The introduction of digital electronics and fly-by-wire controls on aircraft has enabled active Gust Load Alleviation (GLA) to reduce the peak stresses on the airframe produced by any given gust. This conceivably allows some reduction of the specified maximum load factor N_{\max} which the aircraft can withstand without structural failure. Figures 13 and 14 show the fuel burn versus specified maximum load factor for the B737 and B777 class aircraft. The effect is qualitatively similar to that produced by an increase in allowable stress, although now the benefits are smaller because only the primary wing structure is affected by N_{\max} . The fuselage structure is sized by pressurization and landing-impact loads, which are held fixed as the load factor is varied. The tail structure is sized by maximum airloads at a specified never-exceed speed, which is also held fixed here.

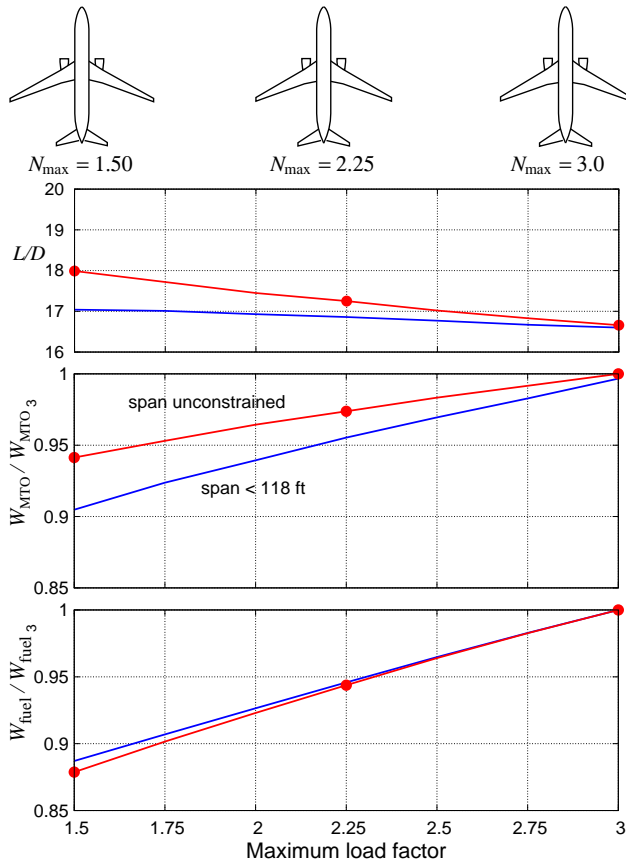


Fig. 13 Optimum B737 class aircraft parameters versus specified maximum load factor.

Engine pressure ratio and turbine materials

Turbofan engine technology has been the subject of continuous intense research and development since the 1950's, as outlined by Koff.¹⁷ NASA's UEET program¹⁸ is a relatively recent example.

Two measures of engine technology are the overall pressure ratio (OPR), and the turbine inlet total temperature T_{t4} . The latter is mainly limited by the

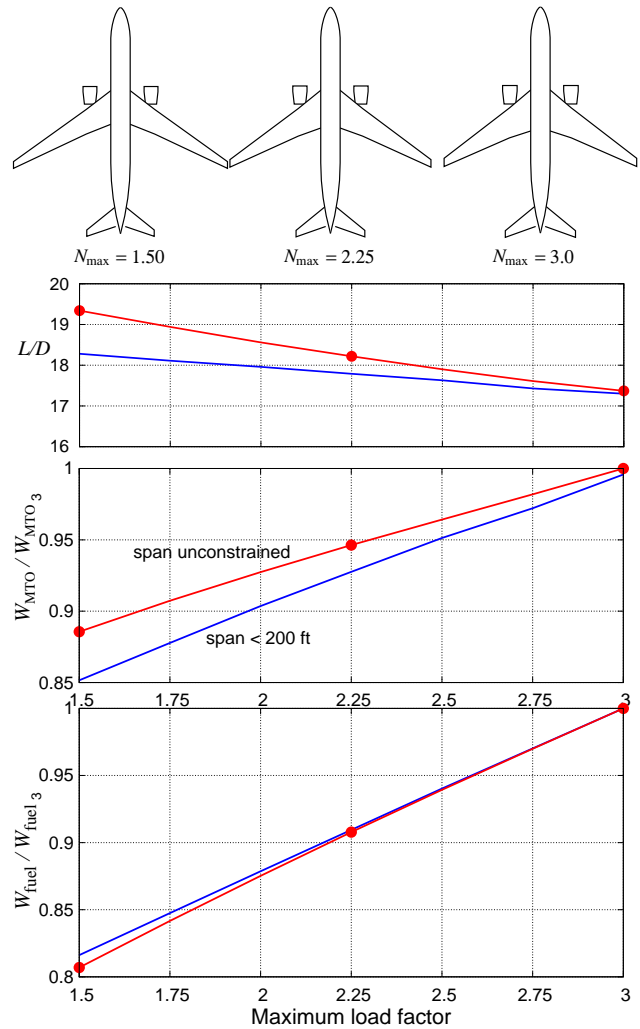


Fig. 14 Optimum B777-class aircraft parameters versus specified maximum load factor.

allowable turbine metal temperature T_{metal} and the turbine-cooling mass flow and effectiveness.

A large OPR naturally produces decreases in $TSFC$ via the ideal Brayton-cycle thermal efficiency relation

$$\eta_T = 1 - 1/OPR^{(\gamma-1)/\gamma} \quad (8)$$

while a large T_{t4} or T_{metal} increases the engine core's power/weight ratio, and thus reduces the engine weight for a given thrust requirement. In the presence of material thermal constraints the two parameters are also coupled in that an increase in OPR also increases the compressor discharge temperature T_{t3} , which in turn reduces the maximum permissible energy input, i.e. temperature rise $T_{t4} - T_{t3}$ across the combustor, and thus limits the core power.

As outlined above, changes in OPR and T_{metal} have a complex influence on the $TSFC$ and thrust/weight ratio, so that the overall engine+airplane system's response to these parameters is quite involved. The overall effect is quantified in Figure 15, which shows the fuel burn versus turbine blade metal temperature, for a range of OPR values. The lowest values

$T_{\text{metal}} = 1200 \text{ K}$, $OPR = 30$ roughly correspond to the CFM56 engine technology from the 1980's which is used on the baseline B737-class aircraft. More modern engines such as the GE90 have $OPR \approx 40$. The extreme $T_{\text{metal}} = 1500 \text{ K}$ is not realistic for existing common superalloys, but might be feasible with future ceramic materials.

The bottom of Figure 15 shows that for any given T_{metal} , there is an optimum OPR value which minimizes fuel burn. For example, at $T_{\text{metal}} = 1250 \text{ K}$ the optimum value is $OPR = 45$. Increasing OPR above this optimum will still decrease $TSFC$, but it will also decrease the engine power due to a smaller available combustor temperature rise. This must be compensated by growing the engine, which adds weight and nacelle drag, offsetting any $TSFC$ reductions.

Figure 15 also shows the takeoff and cruise optimum T_{t4} values, and corresponding turbine cooling mass flow ratio. The surprising result is that these are not monotonic with increasing T_{metal} . Taking the $OPR = 35$ case as an example, we see that as T_{metal} is increased from 1300 K to 1450 K, the optimum gas temperatures stay roughly constant, or even decrease slightly, and instead the cooling mass flow ratio is decreased. This counterintuitive result is from the optimizer exploiting the interactions of the engine and airplane characteristics while being subjected to field-length and climb-gradient constraints. In the middle T_{metal} range where T_{t4} does not increase, it is evidently more effective to reduce fuel burn by reducing the losses of the cooling flow in cruise than by reducing engine weight via larger T_{t4} at takeoff.

Field Length

Airport congestion is a worldwide problem which is expected to get worse with the forecast increases in passenger air traffic. A possible proposed solution¹⁵ is to expand airline operations into smaller airfields surrounding major hubs and metropolitan areas. A limitation of this solution is that these airports have shorter runways, typically 3000–6000 ft., which sets a field-length constraint on future aircraft. Since a shorter field length necessarily increases the minimum mission fuel burn, it is therefore of great interest to quantify this short-field fuel penalty, and to determine how the aircraft must be redesigned to minimize any such penalty.

Figure 16 shows the relative fuel burn and other parameters of interest for the B737-class aircraft versus balanced field length, which is imposed as a constraint in the optimization. The fuel penalty of decreasing the field length from 8000 to 6000 ft is relatively modest, but increases dramatically for still-shorter fields.

The optimizer obtains the field length reduction capability mainly by increasing the wing area and enlarging the engines, in some optimum combination. The wing area increase occurs mostly in the chord, thus

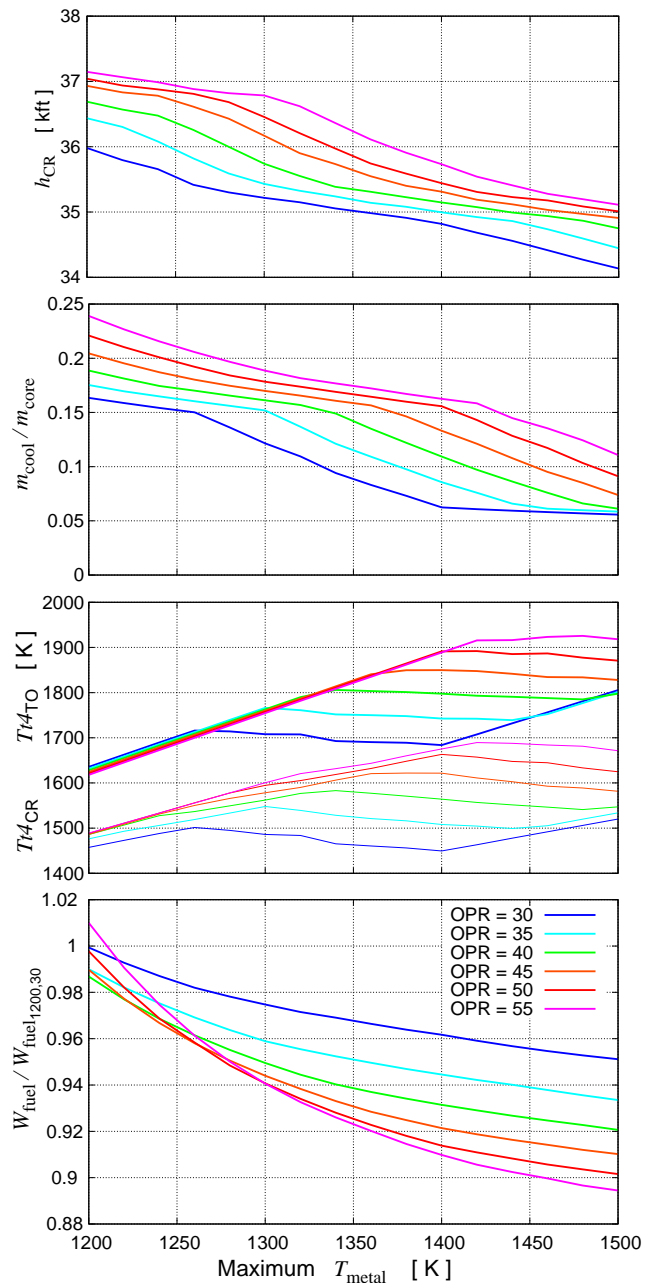


Fig. 15 Optimum B737-class aircraft engine parameters versus maximum turbine metal temperature, for a range of overall pressure ratios.

decreasing the aspect ratio. The optimum engine parameters are also changed, mainly by increasing the fan pressure ratio and decreasing the bypass ratio. All these airframe and engine changes increase the W_{ZF} , D/L , and $TSFC$, and thus produce the increase in the fuel burn as can be seen in the Breguet relation (2).

The field length constraint results in a large excess-lift capability during cruise. This is optimally exploited by an optimum combination of increased start-of-cruise altitude h_{CR} and greatly reduced cruise turbine inlet temperature T_{CR} .

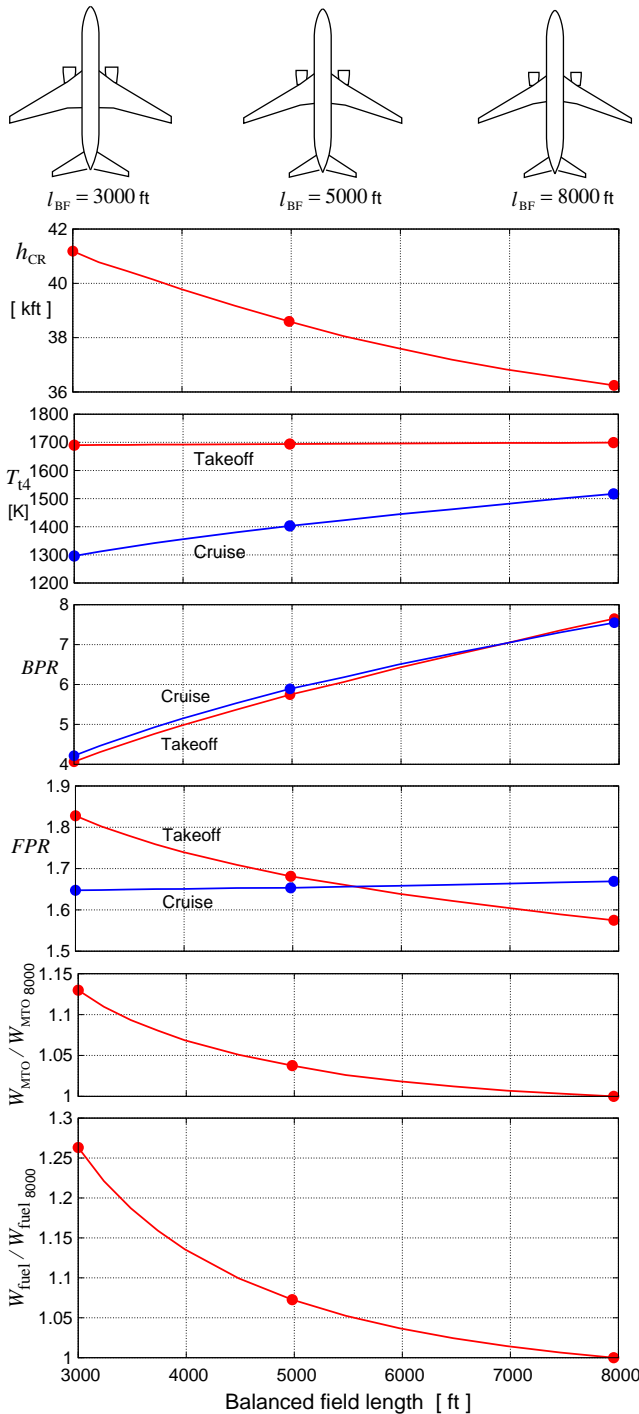


Fig. 16 Optimum B737-class aircraft parameters versus balanced field length.

Stability Margin

The extensive use of fly-by-wire and digital control systems on modern aircraft enables the possibility of using active stability augmentation, commonly referred to as Relaxed Static Stability (RSS).¹⁹ In the present conceptual design study its effect is represented by a reduction in the minimum allowed stability margin, defined for the aftmost-CG passenger loading configuration. The resulting aircraft then has less

fuel burn from a smaller horizontal tail which reduces weight and profile drag. Another contributing factor is less download in cruise at mid-range CG, which reduces trim drag and also shrinks the wing.

Figure 17 shows the fuel burn versus minimum static stability margin, along with other associated parameters of interest. A decrease of 0.05 in margin produces a 1.25% fuel burn reduction, which is not large, but perhaps worth pursuing with a suitable RSS system.

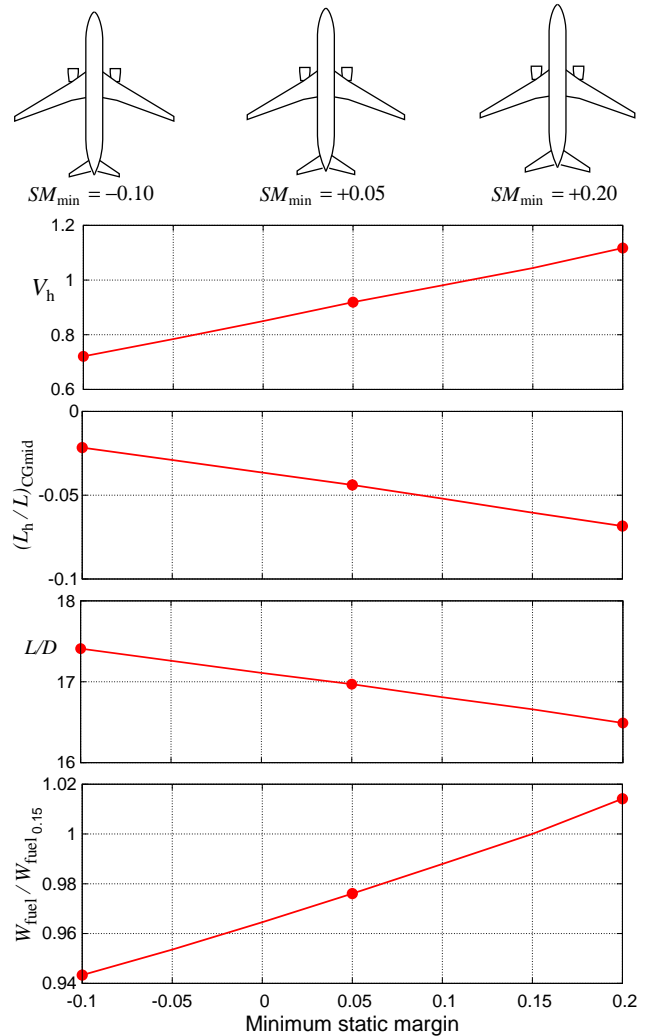


Fig. 17 Optimum B737 class aircraft parameters versus specified minimum (forward-CG) static margin.

Increased seat room allowance

Judging by the complaints about air travel echoed in the media, air travelers are very sensitive to cabin comfort, in particular cramped seating. Alleviating this with a larger-cabin configuration could therefore have a strong marketing benefit, but would inevitably come at a price of increased fuel burn and a larger and more expensive airplane.

To determine the smallest possible fuel burn and gross weight penalties of a larger cabin, the B737-class fuselage shape was progressively grown in diameter to

accommodate 10% and 20% increases in seat width, and then separately stretched lengthwise to accommodate 10% and 20% increases in seat pitch. The global TASOPT optimization was then used to generate optimized aircraft for each of these enlarged fuselage shapes. Figure 18 summarizes the results. Assuming that the width and pitch stretch effects can be superimposed, a 20% increase in both will result in a roughly 15% fuel burn increase. The gross weight would also increase about 8%. The resulting increases in operating and ownership costs and higher ticket prices would of course need to be weighed against the better attractiveness to the air traveler.

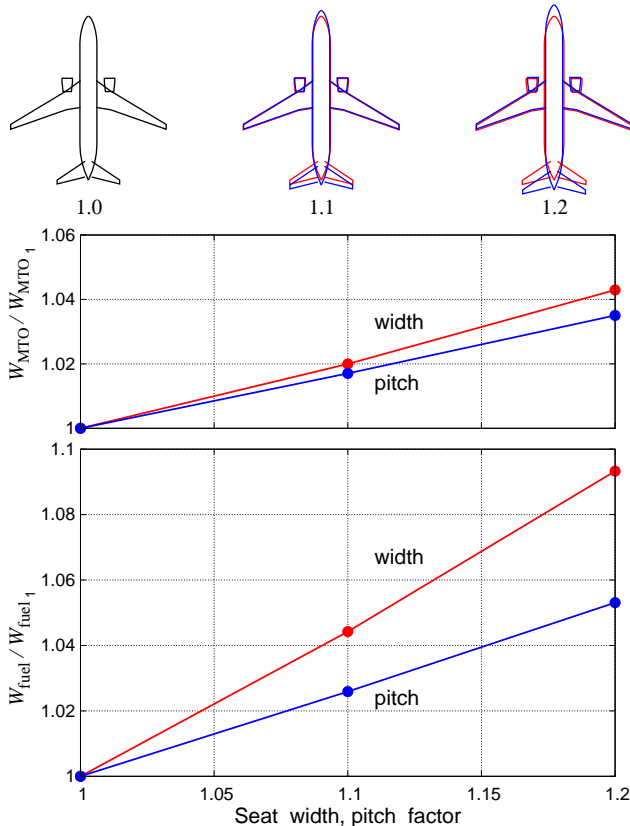


Fig. 18 B737 class aircraft fuel burn and gross weight, versus seat width and pitch.

Skin friction reduction

The profile drag of a transport aircraft in cruise is somewhat more than half of the total drag, and very nearly directly scales with the skin friction integrated over its surface (the pressure-drag component of profile drag actually scales as the displacement thickness, but this itself scales as the skin friction). Because of their great potential payoff in increased range or decreased fuel burn, techniques for reducing skin friction have been extensively pursued for many decades. Most of the effort has been focused on either small-scale streamwise surface ridges or “riblets”, or alternatively on partial laminar flow. There is a very large body of literature on these topics. For a partial review see

Bushnell.⁵

Riblets

Riblets have long been known to be effective for drag reduction in near-zero pressure gradients, as investigated first by Liu et al,²⁰ and subsequently by many others. Their effectiveness was also demonstrated in strong wing-airfoil pressure gradients by McLean et al.²¹ About 5–8% skin friction reduction is achievable by full surface coverage with riblets which are ideally sized for the local Reynolds number. Partial coverage or nonideal sizing will result in smaller friction reductions, or even penalties.

Laminar flow

The possibility of using laminar flow on large jet transports is generally recognized to be extremely difficult, due to their high Reynolds numbers, wing sweep which promotes crossflow instabilities,²² and the relatively “dirty” operating environment. These problems can be overcome with sufficient surface quality and judicious application of Laminar Flow Control (LFC) in the form of distributed suction, as has been demonstrated on a retrofitted Boeing 757 wing in flight.²³ Joslin²⁴ discusses the relevant technology issues. Whether an LFC system is economically viable on an operational airplane is still an open question.

Laminar flow on transonic wings introduces many new design tradeoffs and complications. For example, the weak adverse pressure gradient on an ideal transonic airfoil must be moderated to allow laminar flow, causing loss of lift as sketched in Figure 19. This tradeoff has been examined by Fujino et al.²⁵ Also, laminar

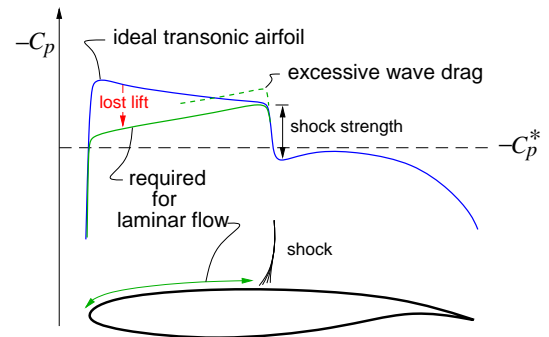


Fig. 19 Slight favorable pressure gradient needed for laminar flow conflicts with ideal transonic pressure distribution, resulting in loss of lift in the presence of a maximum shock strength constraint.

flow is incompatible with leading edge slats, so less effective systems like Kruger flaps are required.

Since laminar flow adversely impacts both the transonic cruise wave drag and possibly also the available $C_{L_{max}}$ for takeoff and landing, it makes the overall aircraft system optimization considerably more complicated, especially at the conceptual design stage. Fully accounting for all such tradeoffs is somewhat beyond the scope of the present conceptual design study.

Simple friction scaling

The focus here is to only estimate the impact on fuel burn of any modest skin friction reduction, however it is obtained. The effect is represented in TASOPT by applying an ad-hoc scaling factor f_{cf} to the skin-friction correlations used in its profile drag predictions.

For representing riblets on a fuselage, the simple friction scaling is deemed reasonable. For riblets on a wing, it does not address the possibility of redesigning the airfoils to fully exploit the healthier boundary layers which result from the riblets, so that here the friction scaling approach might be conservative.

For representing laminar flow, the simple scaling is less realistic overall, since there are now many other interacting effects as discussed above. Nevertheless, it is still considered useful as a best-case indicator of plausible fuel savings which might be achieved. Also of interest, as with the other parameters, is how the engine and operation should be redesigned to best exploit any given skin friction reduction.

To determine the possibly different impacts of reducing friction on the fuselage and the wing, separate TASOPT calculations were performed for these two cases. The results are summarized in Figure 20. The

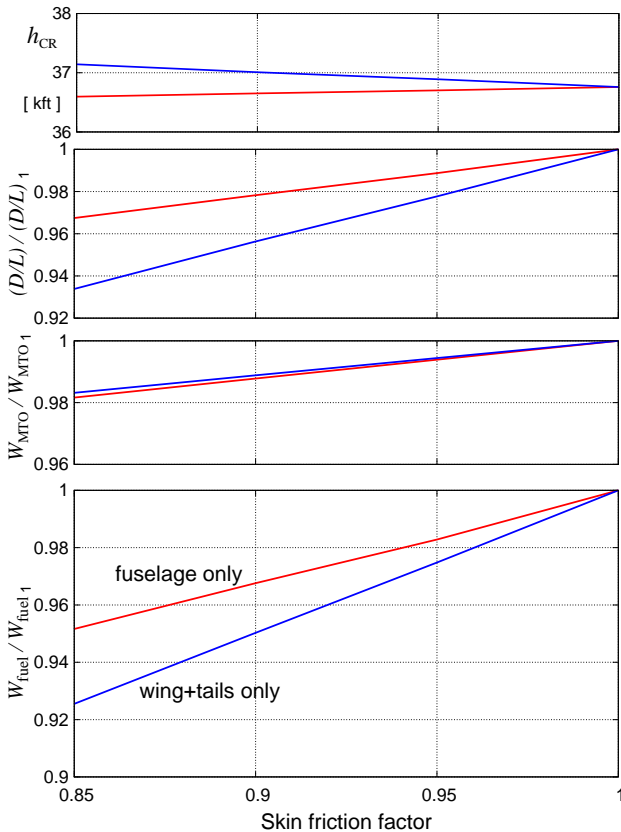


Fig. 20 B737-class aircraft parameters versus skin friction factor.

benefit is larger for friction reduction on the wing and tail surfaces, simply because they have a larger fraction of the total profile drag. It's interesting to note that reducing friction on the wing and tail surfaces in-

creases the optimum altitude, while reducing friction on the fuselage decreases it very slightly. This is consistent with the optimum-altitude tradeoffs discussed earlier.

If the entire surface were covered with optimum riblets with a $f_{cf} = 0.93$ friction factor, the fuselage and surface benefits together would produce a 6% fuel savings. Laminar flow could potentially produce much larger savings, but no overall-savings estimates will be attempted here, since numerous other factors and interactions must be also considered as discussed above.

Alternative Configurations

The conventional low-wing monoplane configuration with wing-mounted engines has been the norm for commercial transport aircraft since the development of the Boeing 707 in the 1950's. The major variation has been the engine placement, as on the B727 and DC9, but the cantilever low wing has persisted. Numerous studies have been conducted into alternative configurations, for example

- the Blended Wing Body (BWB) of Liebeck,²⁶
- the C-wing of McMasters and Kroo,²⁷
- the Joined Wing of Wolkovitch,²⁸
- the Strut-Braced Wing (SBW) of Pfenninger,²⁹
- the author's D8 concept,^{15,30}

and many others. It is far beyond scope to examine and compare all these here. One practical reason is that the TASOPT model uses simple beam theory for its structural models. Hence it is restricted to a wing-tube airplane topology, and cannot be applied to the BWB, C-wing, and Joined-Wing concepts. However, it does apply to the SBW and the D8 concepts, which will be examined here.

Strut-Braced Wing

The SBW concept uses an external strut for wing bending moment relief, which enables some combination of reduced structural weight, larger span, and thinner airfoil. These should overcome the added weight and drag of the strut, resulting in a net reduction in fuel burn.

Many complications arise in the SBW concept, the major ones being strut buckling under negative loads, reduction of fuel volume, aeroelasticity, load paths from landing gear to wing, and crash safety of the high wing above the cabin. Most of these have been addressed by the Truss-Braced Wing,³¹ which is a generalization of the SBW. Here, the focus will be on finding the best SBW airplane+engine+operation for minimum fuel burn as for the other parameter studies. However, complications and associated weight penalties from negative loading requirements, crash-worthiness, and aeroelasticity are ignored. Hence the results here are likely to be optimistic, and should be taken only as a bound on the fuel burn reductions achievable with a single-strut configuration.

Since a strut-braced wing is differently affected by airfoil thickness than the cantilever wing, it is expected to have different Mach/sweep/thickness tradeoff characteristics. For this reason the optimization was performed over a range of cruise Mach numbers like in the earlier cruise-Mach study. The results are summarized in Figure 21. In addition to the unconstrained-span case, two different span constraint cases were calculated: i) span limited to 132 ft which is the optimum unconstrained span for the SBW at $M_{CR}=0.8$, and ii) span limited to 118 ft which is the optimum unconstrained span for the cantilever case $M_{CR}=0.8$, which is shown in Figure 9 and replotted here for comparison.

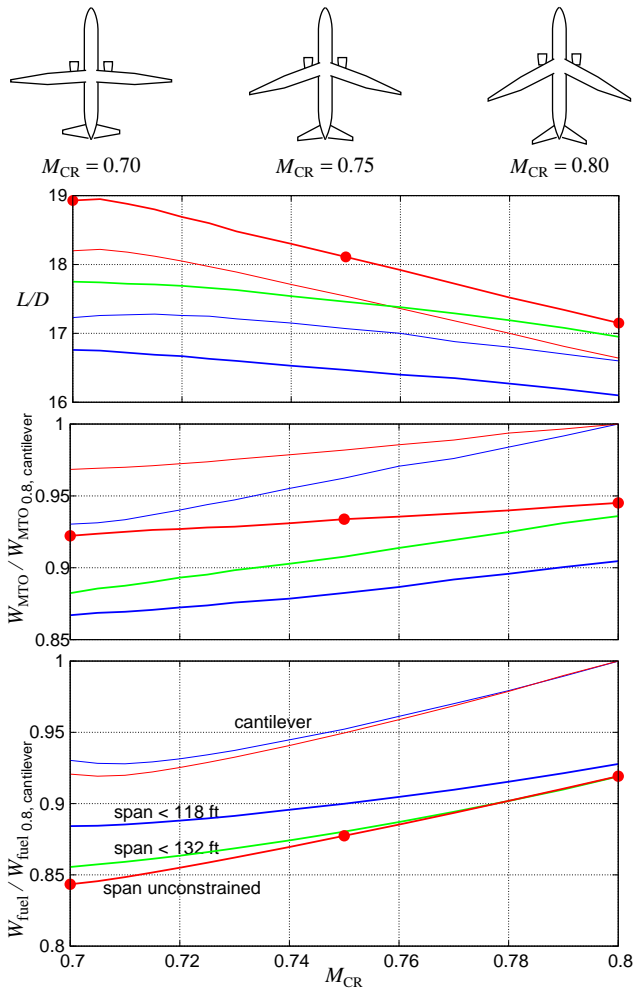


Fig. 21 Strut-braced B737-class aircraft parameters, versus cruise Mach number.

The unconstrained-span SBW configuration appears to offer 8% fuel savings relative to the cantilever configuration. For the constrained-span SBW the savings become 7% at $M_{CR}=0.8$, and 4% at $M_{CR}=0.7$. These savings are attractive, but would need to be examined more closely in light of the potential complications with the SBW configuration discussed above.

D8 Configuration

The D8 configuration was the result of an N+3 study,¹⁵ and was further described by Drela.³⁰ This is a B737-class aircraft with a wide twin-aisle fuselage with upturned nose. Two variants are diagrammed in Figure 22.

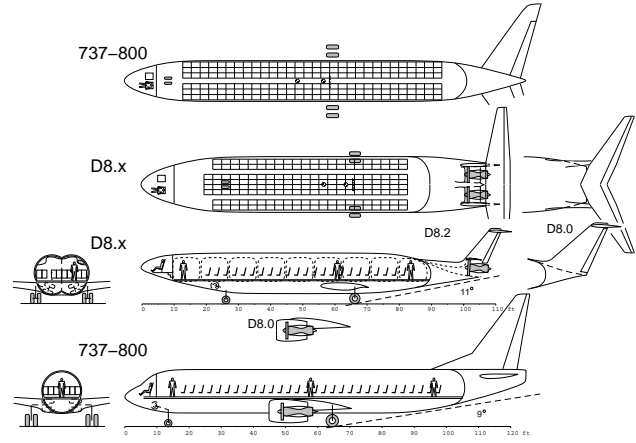


Fig. 22 D8 fuselage on the D8.0 and D8.2 variants, compared with a B737-800 fuselage.

Compared to the conventional B737 fuselage, the main features of the D8 fuselage which produce its fuel savings are:

- increased fuselage carryover lift $C_{L_{fuselage}}$
- less-negative wing-body pitching moment $C_{M_{ac}}$
- smaller CG travel Δx_{cg} due to the shorter cabin
- larger tail effectiveness $\partial c_{\ell_h} / \partial C_L$ at the high location
- lighter two-point supported horizontal tail

The relevant parameter values are compared in Table 3. Their effects on the aircraft are:

- larger fuselage lift correspondingly shrinks the exposed wing area by 6%
- the required horizontal tail area shrinks by 20%
- the tail download in cruise is less negative by 3% of aircraft weight, which further shrinks the wing by another 3%

Table 3 Tail-sizing and tail-load parameter comparison.

Aircraft	$C_{L_{fuselage}}/C_L$	$C_{M_{ac}}$	$\Delta x_{cg}/\bar{c}$	$\partial c_{\ell_h} / \partial C_L$
B737	0.128	-0.1665	0.586	0.36
D8.0	0.195	-0.0825	0.507	0.41

The flat rear D8 fuselage enables a flush-mounted engine installation on the D8.2 variant, with Boundary Layer Ingestion (BLI) of about 40% of the fuselage's boundary layer. The BLI gives 6–8% additional fuel burn reduction, depending on the allowance made for fan efficiency degradation from ingesting the distorted flow. The D8.0 and D8.2 top views are shown in Figure 23. Optimization by TASOPT produces the key parameters and predicted performance listed in Table 4, along with the values for the optimized-B737

baseline. The structural material properties, load factors, and engine technology parameters are specified to be the same for all three airplanes, so the differences are due to configuration alone.

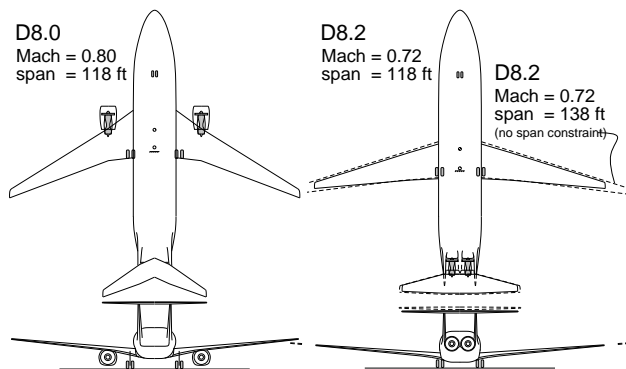


Fig. 23 D8.0 and D8.2 configuration top views.

Table 4 Key parameters of B737, D8.0, and D8.2 configurations, all optimized by TASOPT for minimum W_{fuel} . Baseline weight values are $W_{\text{MTO}} = 162319$ lb and $W_{\text{fuel}} = 35889$ lb.

	M	C_L	L/D	span [ft]	$W_{\text{MTO}}^{\text{frac}}$	$W_{\text{fuel}}^{\text{frac}}$
B737	0.80	0.559	16.33	118	1.000	1.000
D8.0	0.80	0.567	16.39	118	0.894	0.882
D8.2	0.72	0.699	18.32	118	0.775	0.671
D8.2	0.72	0.688	19.84	138	0.815	0.658

If categorized by its wing-mounted engines and typical cruise Mach, the D8.0 is a relatively conventional transport airplane. Nevertheless, it is predicted to produce a 12% fuel savings compared to the optimized-B737 baseline, this being entirely the result of the D8 fuselage and tail characteristics listed in Table 3 which shrink the wing and tail surfaces.

The D8.2, with its low-sweep wing and slower cruise, and its rear BLI engines, is a more novel configuration. In addition to the fuselage's benefits, the D8.0 also exploits the cumulative effects of the reduced Mach number, BLI, shorter landing gear, smaller vertical tails allowed by the small engine-out yaw moments, and other miscellaneous features. The net result is a quite large 33% fuel burn reduction.

Concluding Remarks

This paper has presented calculations of sensitivities of fuel burn to a variety of key design parameters of tube and wing transport aircraft. The parameters encompass materials technology, engine technology, and operations, and were selected on the basis of their expected strong influence on fuel burn. The quantification of these sensitivities gives guidance for where research efforts might be directed so as to have significant impact on the fuel economy of future transport aircraft.

Acknowledgments

The author would like to thank Doug McLean (Boeing, ret.), Ed Greitzer (MIT), and Wesley Lord (Pratt&Whitney) for their helpful critique and suggestions.

References

- ¹NASA Aeronautics Research Mission Directorate. Fundamental Aeronautics Program: Subsonic Fixed Wing, Sep 2009. <http://www.aeronautics.nasa.gov/fap/>.
- ²NASA Aeronautics Research Mission Directorate. N+3 Program, June 2010. http://www.nasa.gov/topics/aeronautics/features/future_airplanes.html.
- ³J.I Hileman, J.B. Katz, J. Mantilla, and G. Fleming. Payload fuel energy efficiency as a metric for aviation environmental performance. Proceedings of the 26th ICAS Conference, Anchorage, AK, Sep 2008.
- ⁴R.S. Shevell. *Fundamentals of Flight, 2nd Edition*. Prentice Hall, Englewood Cliffs, New Jersey, 1989.
- ⁵D.M. Bushnell. Aircraft drag reduction — a review. *Journal of Aerospace Engineering*, 217:1–18, 2003.
- ⁶J. Roskam. *Airplane Design*. DAR Corporation, Lawrence, Kansas, 2000.
- ⁷E. Torrenbeek. *Synthesis of Subsonic Airplane Design*. Delft University Press, 1988.
- ⁸D.P. Raymer. *Aircraft Design: A Conceptual Approach*. AIAA Education Series. AIAA, 1992.
- ⁹S. Jayaram, A. Myklebust, and P. Gelhausen. ACSYNT — A standards-based system for parametric computer aided conceptual design of aircraft. AIAA Paper 92-1268, Feb 1992.
- ¹⁰W.H. Mason and T.K. Arledge. ACSYNT aerodynamic estimation — An examination and validation for use in conceptual design. AIAA Paper 93-0973, Feb 1993.
- ¹¹M.B. Knapp. Applications of a nonlinear wing planform design program. Master's thesis, MIT, Aug 1996.
- ¹²S. Wakayama. *Lifting Surface Design Using Multidisciplinary Optimization*. PhD thesis, Stanford, June 1994.
- ¹³I. Kroo. PASS, Program for Aircraft Synthesis Studies. Software Package, Desktop Aeronautics, Palo Alto, CA, 2005.
- ¹⁴M. Drela. N+3 Aircraft Concept Designs and Trade Studies — Appendix. Technical Report NASA CR-2010-216794/VOL2, NASA, 2010.
- ¹⁵E.G. Greitzer. N+3 Aircraft Concept Designs and Trade Studies. Technical Report NASA CR-2010-216794/VOL1, NASA, 2010.
- ¹⁶F. Chang. *Structural health monitoring: The demands and challenges*. CRC Press, 1999.
- ¹⁷B.L. Koff. Gas turbine technology evolution: A designer's perspective. *Journal of Propulsion and Power*, 20(4):577–595, Jul–Aug 2004.
- ¹⁸NASA Glenn Research Center. Ultra-Efficient Engine Technology Program, Jan 2010. <http://www.grc.nasa.gov/WWW/RT/RT2000/2000/2010shaw.html>.
- ¹⁹S.M. Sliwa. Economic evaluation of flying-qualities design criteria for a transport configured with relaxed static stability. Technical Report TP-1980-1760, NASA, 1980.
- ²⁰S.J. Liu, C.K. and Kline and J.P. Johnston. An experimental study of turbulent boundary layer on rough walls. Report MD-15, Stanford U. Dep. Mech. Eng., July 1966.
- ²¹J.D. McLean, D.N. George-Falvy, and P.P. Sullivan. Flight-test of turbulent skin friction reduction by riblets. Proceedings of International Conference on Turbulent Drag Reduction by Passive Means, Royal Aeronautical Society, London, 1987.
- ²²H.L. Reed and D. Saric, W.S. and Arnal. Linear stability theory applied to boundary layers. *Annual Reviews of Fluid Mechanics*, 28, 1996.

²³Boeing Commercial Aircraft Group. High Reynolds number hybrid laminar flow control (HLFC) flight experiment. Technical Report CR-1999-209324, NASA, 1999.

²⁴R.D. Joslin. Overview of laminar flow control. Technical Report TP-1998-208705, NASA, 1998.

²⁵M. Fujino, Y. Yoshizaki, and Y. Kawamura. Natural laminar-flow airfoil development for a lightweight business jet. *Journal of Aircraft*, 40(4):609–615, Jul-Aug 2003.

²⁶R. Liebeck. Design of the Blended Wing Body subsonic transport. *Journal of Aircraft*, 41(1), Jan 2004.

²⁷J.H. McMasters and I. Kroo. Advanced configurations for very large subsonic transport airplanes. Technical Memorandum TM 109154, NASA, Sept 1994.

²⁸J. Wolkovitch. The joined wing: An overview. *Journal of Aircraft*, 23(3), Mar 1986.

²⁹W. Pfenninger. Some thoughts on the design of large global range lift transport airplanes. In *Special Course on Concepts for Drag Reduction*. AGARD, 1976.

³⁰M. Drela. Development of the D8 Transport Configuration. AIAA Paper 2011-3970, June 2011.

³¹O. Gur, M. Bhatia, W.H. Mason, J.A. Schetz, R.K. Kapania, and T. Nam. Development of a framework for truss-braced wing conceptual MDO. *Struc. Multidisc. Optim.*, 44:277–298, 2011. Also appeared as AIAA paper 2010-2754.